Strain sensitivity of band gaps of Sn-containing semiconductors

Li, Hong; Castelli, Ivano Eligio; Thygesen, Kristian Sommer; Jacobsen, Karsten Wedel

Published in:
Physical Review B

Link to article, DOI:
10.1103/PhysRevB.91.045204

Publication date:
2015

Document Version
Publisher's PDF, also known as Version of record

Strain sensitivity of band gaps of Sn-containing semiconductors

Hong Li, Ivano E. Castelli, Kristian S. Thygesen, and Karsten W. Jacobsen*

Center for Atomic-scale Materials Design, Department of Physics, Technical University of Denmark, DK-2800 Kongens Lyngby, Denmark

(Received 18 November 2014; published 22 January 2015)

Tuning of band gaps of semiconductors is a way to optimize materials for applications within photovoltaics or as photocatalysts. One way to achieve this is through applying strain to the materials. We investigate the effect of strain on a range of Sn-containing semiconductors using density functional theory and many-body perturbation theory calculations. We find that the band gaps of bulk Sn oxides with SnO_6 octahedra are highly sensitive to volumetric strain. By applying a small isotropic strain of 2% (−2%), a decrease (increase) of band gaps as large as 0.8 to 1.0 eV are obtained. We attribute the ultrahigh strain sensitivity to the pure Sn *s*-state character of the conduction-band edges. Other Sn-containing compounds may show both increasing and decreasing gaps under tensile strain and we show that the behavior can be understood by analyzing the role of the Sn *s* states in both the valence and the conduction bands.

DOI: 10.1103/PhysRevB.91.045204 PACS number(s): 71.20.Nr

I. INTRODUCTION

The need for more sustainable energy solutions has spawned many efforts in finding materials appropriate for absorption of solar light to be used in either photovoltaics or in solar-to-fuel devices [1]. A key parameter in these materials is the band gap, which sets some limits on how efficient the device can be [2]. The efforts go into discovering entirely new materials as well as optimizing the band-gap and band-edge positions of known materials in many different ways. The modifications may involve strain [3–5], doping [6,7], alloying [8,9], heterogeneous structuring [10], surface ligand passivation [11], or atomically thin layering [12–14]. Strain can be introduced directly in a material by an externally applied stress field, but it also often interplays with other modification mechanisms which indirectly modify the strain. For example, the nanostructuring of a material often leads to interface or surface stresses which because of the small scale can have strong strain effects through the entire material. Recently, Yang *et al.* showed how core/shell nanostructures in CdSe/CdTe systems can lead to significant strain-induced band-gap modification [15].

In this paper, we study the effect of strain on the band gaps for a series of 14 bulk semiconductors, mainly Sn compounds, using density functional theory (DFT) and many-body perturbation theory within the G_0W_0 approximation. A small strain range from −2% to 2% is applied equally on all three dimensions. We find that the band gaps of the Sn oxides with SnO_6 octahedra are ultrasensitive to strain. Rotations of the BO_6 octahedra and induced volume changes are investigated in the four primitive perovskite formula cells ($\sqrt{2} \times \sqrt{2} \times 2$) of $CaSnO_3$ and $CaTiO_3$. Finally, we study strain effects in *A*- and *B*-site alloys for $SrSnO_3$ with Ba and Ti, respectively.

II. COMPUTATIONAL METHODOLOGY

We consider the strain dependence of the band gap in 14 three-dimensional (3D) semiconductors, i.e., ten cubic perovskites among ABO_3 (A = Ca, Sr, Ba or Sn, and B = Sn or Ti) and ABI_3 (A = Cs or CH_3NH_3, and B = Sn or Pb), one rutile SnO_2, two rhombohedral SnS_2 and $SnSe_2$, and one layered perovskite with the Ruddlesden-Popper phase Sr_2SnO_4. All of the structures have octahedral character as part of their geometry. A small strain from −2% to 2% with a step of 0.5% is applied equally in all three dimensions. Four primitive perovskite formula cells ($\sqrt{2} \times \sqrt{2} \times 2$) are constructed to study $CaSnO_3$ and $CaTiO_3$ with rotations of the BO_6 octahedra.

The calculations are all performed using the DFT and many-body perturbation theory code GPAW [16,17] with the projector augmented wave approximation (PAW) implemented. Bulk lattice relaxations are carried out using the Perdew-Burke-Ernzerhof (PBE) exchange-correlation functional called PBEsol [18]. We use a plane-wave cutoff of 800 eV and the Brillouin zones are sampled using a $6 \times 6 \times 6$ Monkhorst-Pack k mesh [19]. The residual force per atom is converged to less than 0.01 eV/Å.

To determine the band structure and band gaps, a denser Γ-centered $10 \times 10 \times 10$ Monkhorst-Pack k-point grid is applied. The electronic band gaps are calculated using the exchange-correlation functional GLLB-SC by Gritsenko *et al.* [20], adapted by Kuisma *et al.* [21] to include the PBEsol correlation for solids (-SC). The GLLB-SC functional includes explicit calculations of the derivative discontinuity added to the Kohn-Sham (KS) band gap to obtain the quasiparticle (QP) gap. A number of studies have shown that the GLLB-SC functional at a minimal computational cost gives reasonable band gaps for oxides and other materials in comparison with experiment and many-body perturbation theory [22–24]. The QP gaps in the G_0W_0 approximation [25] are also calculated for $BaSnO_3$, and $BaTiO_3$ using PBE eigenvalues and wave functions as input. Considering the balance of accuracy and computer time, two approximations are adopted in the G_0W_0 calculations. One is the use of the plasmon pole approximation (PPA) by Godby and Needs for the dielectric function [26], instead of an explicit treatment of the frequency dependence. This kind of PPA model has been demonstrated to agree well with explicit frequency-dependent methods for band gaps [27,28]. The other approximation is based on the observation that increasing the k-mesh grid leads to only a constant shift of

*kwj@fysik.dtu.dk

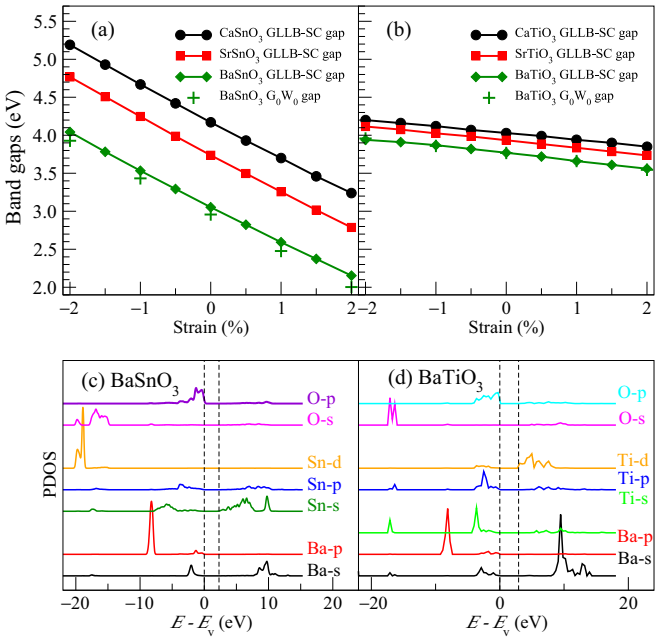

FIG. 1. (Color online) (a),(b) The GLLB-SC and G_0W_0 QP gaps of cubic perovskite ABO_3 (A = Ca, Sr or Ba, and B = Sn or Ti) as a function of strain. (c),(d) The PDOS for (c) $BaSnO_3$ and (d) $BaTiO_3$. The gap indicated here is the KS part of the GLLB-SC QP gap with the top of the valance bands set to zero.

the G_0W_0 QP gaps [25]. Thus, the G_0W_0 QP gaps are obtained by combining the extrapolation to infinite cutoff energy using coarse $4 \times 4 \times 4$ k points and calculation at a low cutoff energy, such as 50 eV, for denser $10 \times 10 \times 10$ k points.

III. RESULTS AND DISCUSSIONS

The calculated GLLB-SC QP band gaps of ABO_3 (A = Ca, Sr or Ba, and B = Ti or Sn) as a function of strain are shown in Figs. 1(a) and 1(b) for B = Sn and B = Ti, respectively. The G_0W_0 QP gaps for $BaSnO_3$ and $BaTiO_3$ for some selected strain values are also shown. The agreement between the GLLB-SC and G_0W_0 QP gaps is clearly good with a deviation of only about 0.1 eV. The strain effect on the $ASnO_3$ series is more remarkable than that of the $ATiO_3$ ones, and the QP gaps all drop linearly with increasing strains from -2% to 2%. The band gaps decrease (increase) dramatically by 0.90–0.95 eV at a small strain of 2% (-2%) for $ASnO_3$, while the drop (increase) for $ATiO_3$ is only 0.18–0.21 eV at the same strain. In particular, the QP gap of $BaSnO_3$ drops from 3.05 to 2.15 eV at a tensile strain of 2%, bringing it into a region relevant for visible light absorption. Our results agree well with recent work on strain effects in $SrSnO_3$ and $BaSnO_3$, where a drop of $\sim$1 eV of the band gap with an increase of the volume by ~ 4 Å^3 (corresponding to $\sim$2% strain) was found [4]. We fit the QP gaps with strains using a linearly functional form: $E_g(x) = E_g(0) + k \times x$, where x is the percent of strain. It is interesting to see that each of the $ASnO_3$ and $ATiO_3$ series have similar slopes, with values of k from -0.47 to -0.49 and -0.087 to -0.098, respectively. To illuminate the mechanism behind the band-gap variation for the two series, we plot the projected density of states (PDOS), for $BaSnO_3$ and $BaTiO_3$ in Figs. 1(c) and 1(d), respectively. The gap indicated here is the KS gap of the GLLB-SC QP gap. We find that all of the valence-band maxima (VBM) can be mainly attributed to the oxygen (O) p states, while the conduction-band minima (CBM) can be attributed to tin (Sn) s states and titanium (Ti) d states for the $ASnO_3$ and $BTiO_3$ series, respectively. The calculations thus suggest that the Sn s-state character plays a major role for the ultrahigh strain sensitivity.

To more generally investigate the strain sensitivity when Sn is involved, we investigate seven other Sn compounds (SnO_2, SnS_2, $SnSe_2$, $SnTiO_3$, $CsSnI_3$, $CH_3NH_3SnI_3$, and Sr_2SnO_4) and also one Pb compound ($CsPbI_3$). The calculated GLLB-SC KS and QP band gaps as a function of strain are shown in Fig. 2(a). We see that the band gaps can both increase and decrease with strain. For all of the systems considered, the strain shows a combined effect on both the KS gap and the derivative discontinuity. In fact, the changes in the KS and the derivative discontinuity parts of the QP gap due to strain are usually proportional to the contribution they have to the QP gap. The most remarkable variation in the gap is seen for SnO_2 and Sr_2SnO_4, where the variation is of the same order of magnitude as was seen for the $ASnO_3$ compounds with a band-gap drop of about 0.8 eV at a strain of 2%. The sensitivity seems to have the same origin as for the $ASnO_3$ compounds since the CBM are dominated by Sn s states for SnO_2 and a combination of Sn and Sr s states for Sr_2SnO_4, as shown in Fig. 2(b) for the case of SnO_2.

The compounds SnS_2 and $SnSe_2$ exhibit a more moderate decrease of the band gap with strain. For these systems, the CBM still exhibits some Sn s-state character; however, it is now mixed with a strong component of S and Se p states for SnS_2 and $SnSe_2$, respectively. This can be seen in the PDOS of SnS_2 in Fig. 2(c). In all of the cases with decreasing band gaps, the VBM are dominated by the anion (O, S, or Se) p states and seem to play a minor role for the variation observed.

The remaining compounds, i.e., $SnTiO_3$, $CsSnI_3$, $CH_3NH_3SnI_3$, and $CsPbI_3$, all exhibit an increase in the band gap as a function of strain. In these compounds, the Sn s states do not come into play at the CBM. For $SnTiO_3$, the CBM is dominated by Ti d states [see Fig. 2(d)], while for $CsSnI_3$ and $CH_3NH_3SnI_3$, the main weight at the CBM comes from the Sn p states and, analogously, for $CsPbI_3$ [Fig. 2(e)], the Pb p states [29]. However, now the VBM can be attributed to a combination of the Sn/Pb s states and the anion p states leading to an increase of the gap with strain.

We verify the role of electronic character of the edge states by calculating the shifts of the edges with strain relative to a common reference taken as the pseudo-Hartree potential close to an atomic core [30]. The shifts of the edges at a strain of 2% for $BaSnO_3$, SnS_2, and $SnTiO_3$ compared to the unstrained situation are given in Table I. We see that for $BaSnO_3$, the large drop in band gap comes from the lowering of the CBM, which in this case is dominated by the pure Sn s states. For SnS_2, the moderate decrease of the band gap is mainly due to the CBM moving down, but the effect is smaller than for $BaSnO_3$ because the CBM here is composed of a mix of Sn s states and S p states. For $SnTiO_3$, the moderate increase of the gap comes from a lowering of the VBM which is associated with a mix of Sn s states and O p states. We thus see that in all cases, the change in band gap can be understood from a downshift

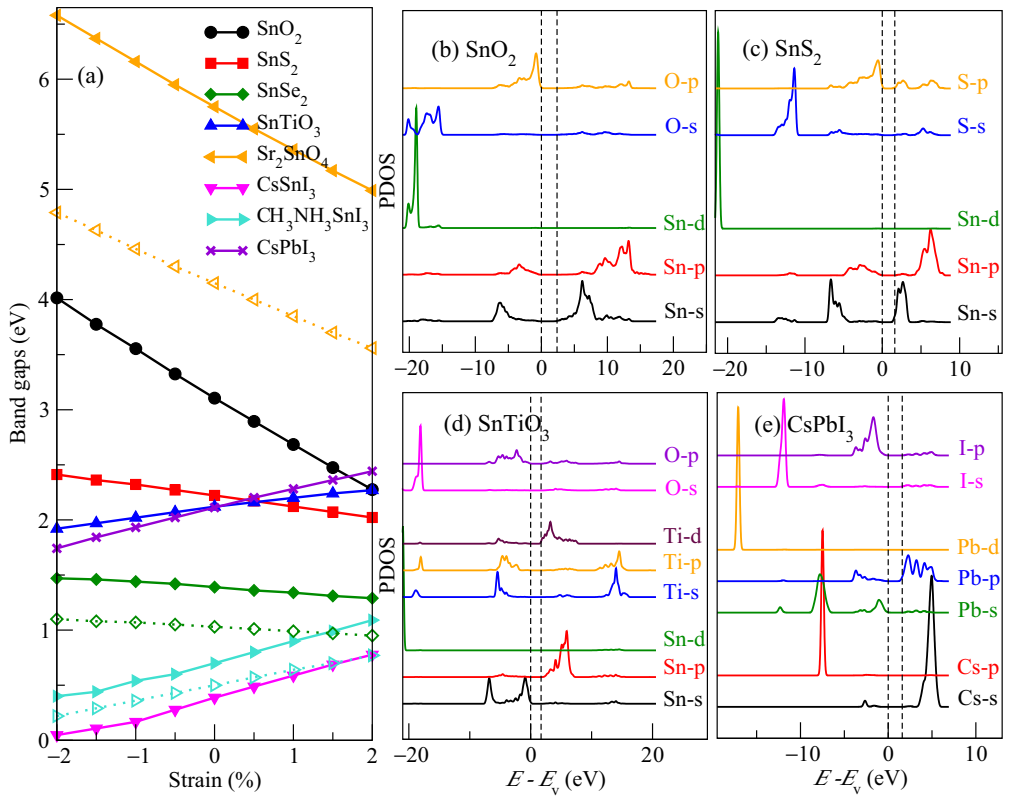

FIG. 2. (Color online) (a) The GLLB-SC KS (dashed lines and open markers) and QP (solid line and full markers) gaps as a function of strains for a selection of 3D semiconductors. (b)–(e) The PDOS for (b) SnO_2, (c) SnS_2, (d) $SnTiO_3$, and (e) $CsPbI_3$. The gap appearing in the PDOS is the KS part of the GLLB-SC QP gap and the top of valence band is set to zero.

of the Sn s states and the effect is particularly large if the Sn s states are not mixed with other states.

Many perovskites (cubic phase space group $Pm-3m$) commonly occur in an orthorhombic form in nature with a space group of $Pbnm$ (i.e., $CaSnO_3$ and $CaTiO_3$), with a unit cell which contain four primitive perovskite formula cells ($\sqrt{2}\times\sqrt{2}\times 2$). Tilts and rotations of the BO_6 octahedra take place and give rise to the lattice reconstruction. The calculated GLLB-SC QP gaps for the orthorhombic $CaSnO_3$ and $CaTiO_3$ are 4.90 and 4.54 eV, enlarged by 0.73 and 0.51 eV, compared to 4.17 and 4.03 eV for the cubic perovskites, respectively.

If the relative positions of the atoms are kept fixed in the reconstructed phase and the lattice parameters are forced to be the ones in the cubic phase, we get GLLB-SC QP gaps of 4.43 and 4.42 eV for $CaSnO_3$ and $CaTiO_3$, respectively. Thus we see that the tilts and rotations of the internal atom coordinates contribute 0.26 and 0.39 eV to the band gaps, while the reconstruction of the lattice contributes 0.47 and 0.12 eV to the enlargement of the orthorhombic $CaSnO_3$ and $CaTiO_3$, respectively.

TABLE I. The shifts of the band edges (in eV) at 2% strain relative to the unstrained situation for $BaSnO_3$, SnS_2, and $SnTiO_3$. The shifts are calculated by taking the pseudo-Hartree potential close to an atomic core as a common reference.

	$BaSnO_3$	SnS_2	$SnTiO_3$
CBM	−0.53	−0.17	−0.01
VBM	0.18	−0.03	−0.14

To investigate the reconstruction effects on the band gap further, we make a simple model of the reconstruction by just rotating the two oxygen layers of each octahedron gradually in opposite ways around the z axis (in tetragonal symmetry), as shown in Fig. 3(a). The displacement of the two oxygen layers is along the primitive unit cell vectors in the xy plane, and we define a displacement parameter as the ratio between the displacement of one of the oxygen atoms from its original ideal position and the primitive lattice constant. The GLLB-SC QP gaps of the deformed $CaSnO_3$ and $CaTiO_3$ in the $\sqrt{2}\times\sqrt{2}\times 2$ unit cell are shown in Fig. 3(b) for the two different cases of optimized volume and a fixed volume. It is clear to see that the change of volume dominates the increase of the band gap in $CaSnO_3$, as also found by Singh *et al.* [4], while for the $CaTiO_3$ the change of band gap is dominated by the rotation of the octahedra. The difference between the two systems arises from the $CaSnO_3$ having the CBM dominated by the more delocalized Sn s states, which gives a high-volume sensitivity [4], while the CBM of $CaTiO_3$ is dominated by Ti d states where directional bonding plays a significant role.

As seen above, the $SrSnO_3$ exhibits a very strong strain dependence of the gap. To which extent will such a feature remain if alloying is applied? To study this, we consider two examples of 50% substitution of Ba in the A site

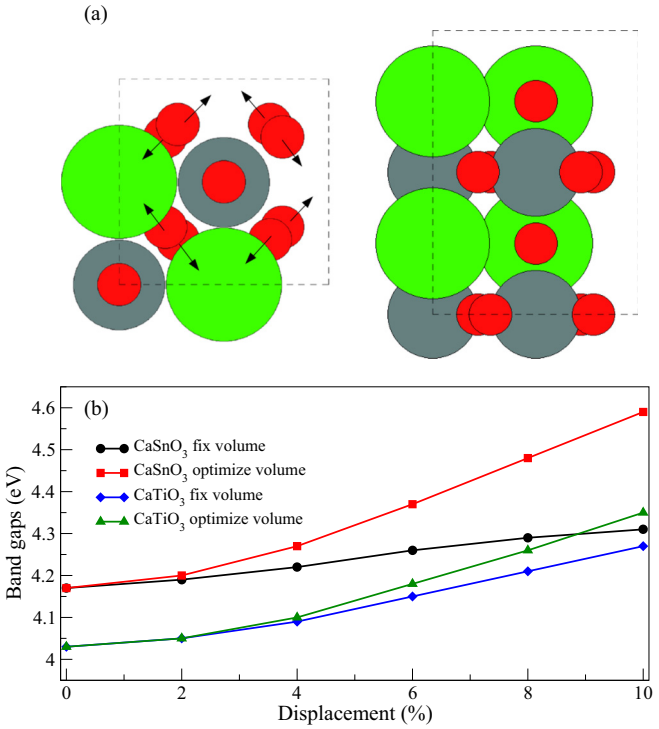

FIG. 3. (Color online) (a) Illustration of how the rotation of the octahedra in $CaSnO_3$ and $CaTiO_3$ is applied (seen from two directions). The displacement measures the movement of one of the oxygen atoms. Green ball: Ca; gray ball: Sn/Ti; red ball: O. (b) The calculated GLLB-SC QP gaps as a function of oxygen displacement shown for both fixed and optimized volumes.

(replacing Sr) or Ti in the *B* site (replacing Sn). For simplicity, we just take the average lattice parameters of each two perovskites as the equilibrium lattice constant. The GLLB-SC QP gaps as a function of volumetric strain for the two alloys $(Sr_{0.5}Ba_{0.5})SnO_3$ and $Sr(Sn_{0.5}Ti_{0.5})O_3$ and their PDOS are shown in Figs. 4(a), 4(b), and 4(c), respectively. We find that the *A*-site alloying does not break the strong strain dependence of the band gap, while the substitution at the *B* site leads to a much weaker dependence. This dependence supports the previous explanations of the importance of the Sn *s* states at the CBM as an indicator of strong strain dependence because, as can be seen in the PDOS in Figs. 4(b) and 4(c), the CBM of the $(Sr_{0.5}Ba_{0.5})SnO_3$ system is dominated by the Sn *s* states, while in $Sr(Sn_{0.5}Ti_{0.5})O_3$ the CBM character has changed to Ti *d* states. The high strain sensitivity of the band gap of $(Sr_{0.5}Ba_{0.5})SnO_3$ is in good agreement with experimental studies of $(Ba_{1-x}Sr_x)SnO_3$ thin films epitaxially grown on MgO substrates, where tuning the coverage of Sr from $x = 0$ to 1 gradually decreases the out-of-plane lattice parameter by $\sim$2% and leads to an increase of the band gap by 0.77 eV [8].

To conclude, the alloying proportion of the *A*-site atom (Ba) in $SrSnO_3$ tunes the band gap not through directly affecting the electronic character of the bands but mainly through the induced change of volume. A similar volume effect can be seen in $ASnO_3$ (A = Ca, Sr, and Ba) with the increasing volume of the *A*-site atom. Importantly, this also provides a way of tuning the band gap in the organic perovskites, as can be seen by comparing $CsSnI_3$ and $CH_3NH_3SnI_3$, where the larger *A*-site

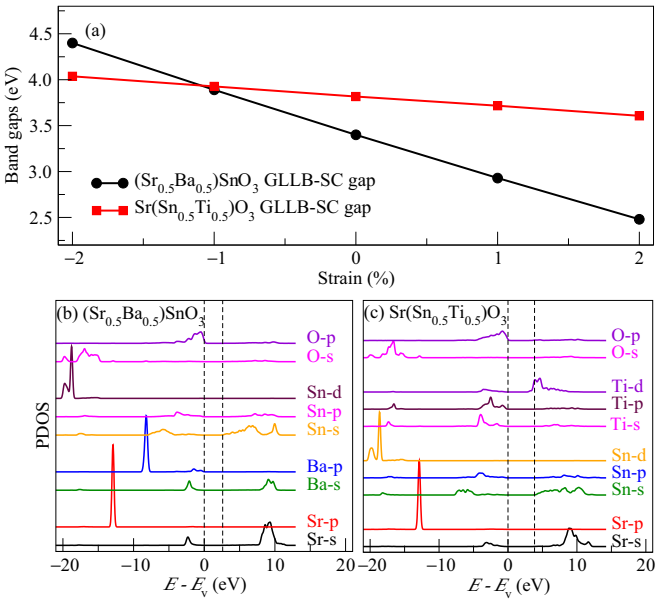

FIG. 4. (Color online) (a) The GLLB-SC QP gaps with strains for alloys. (b),(c) The PDOS for (b) $(Sr_{0.5}Ba_{0.5})SnO_3$ and (c) $Sr(Sn_{0.5}Ti_{0.5})O_3$. The gap indicated here is the KS part of the GLLB-SC QP gap with the top of the valance band set to zero.

molecule CH_3NH_3 leads to a larger volume and therefore a larger gap [31].

IV. CONCLUSION

We have investigated the possibilities of using strain to modify the band gaps of a range of compounds containing tin based on electronic structure calculations. The increase or decrease in the QP band gap is generated by the variation that the strain induces in both the KS and the derivative discontinuity contributions to the QP gap. The sensitivity of the band gaps to strain is quite different depending on the material and the differences can be systematized by considering the electronic states which play a role for the band-edge states. A very high strain sensitivity was observed for the compounds where the CBM states could be attributed to mainly Sn *s* states possibly in combination with other *s* states. A clear decrease in the band gaps as a function of increasing volumetric strain was thus observed for $ASnO_3$ (A = Ca, Sr, Ba), SnO_2, and $SrSnO_4$. For the cases SnS_2 and $SnSe_2$, where the CBM states involve a combination of Sn *s* states and anion *p* states, a more moderate decrease of the band gap with increasing strain was observed. For the $SnTiO_3$ and the class of halide perovskites $CsSnI_3$, $CH_3NH_3SnI_3$, and $CsPbI_3$, the effect has the opposite sign so that a tensile strain leads to an increased band gap, and this behavior can be traced to the VBM now being attributed to a combination of Sn *s* states and anion *p* states. The large sensitivity to volumetric strain for materials with the CBM dominated by Sn *s* states was also confirmed for alloy systems where $(Sr_{0.5}Ba_{0.5})SnO_3$ shows a large decrease of the band gap with increasing strain, while $Sr(Sn_{0.5}Ti_{0.5})O_3$, where the CBM is dominated by Ti *d* states, shows a much weaker dependence. Recent experimental investigations of $(Ba_{1-x}Sr_x)SnO_3$ thin films expitaxially grown on MgO substrates confirm the high strain sensitivity of the band gap in this type of system.

ACKNOWLEDGMENTS

The authors acknowledge support from the Catalysis for Sustainable Energy (CASE) initiative funded by the Danish Ministry of Science, Technology and Innovation and from the Center on Nanostructuring for the Efficient Energy Conversion (CNEEC) at Stanford University, an Energy Frontier Research Center founded by the U.S. Department of Energy, Office of Science, Office of Basic Energy Sciences under Award No. DE-SC0001060.

[1] M. G. Walter, E. L. Warren, J. R. McKone, S. W. Boettcher, Q. Mi, E. A. Santori, and N. S. Lewis, Solar water splitting cells, Chem. Rev. **110**, 6446 (2010).

[2] W. Shockley and H. J. Queisser, Detailed balance limit of efficiency of *p-n* junction solar cells, J. Appl. Phys. **32**, 510 (1961).

[3] S. Yang, D. Prendergast, and J. B. Neaton, Nonlinear variations in the electronic structure of II–VI and III–V wurtzite semiconductors with biaxial strain, Appl. Phys. Lett. **98**, 152108 (2011).

[4] D. J. Singh, Q. Xu, and K. P. Ong, Long-term superelastic cycling at nano-scale in Cu-Al-Ni shape memory alloy micropillars, Appl. Phys. Lett. **104**, 011901 (2014).

[5] M. Taib, M. Yaakob, A. Chandra, A. K. M. Arof, and M. Yahya, Effect of pressure on structural, electronic and elastic properties of cubic (Pm3m) $SnTiO_3$ using first principle calculation, Adv. Mater. Res. **501**, 342 (2012).

[6] F. Yang, N.-N. Yan, S. Huang, Q. Sun, L.-Z. Zhang, and Y. Yu, Zn-Doped CdS nanoarchitectures prepared by hydrothermal synthesis: Mechanism for enhanced photocatalytic activity and stability under visible light, J. Phys. Chem. C **116**, 9078 (2012).

[7] F. Wang, C. Di Valentin, and G. Pacchioni, Doping of WO_3 for photocatalytic water splitting: Hints from density functional theory, J. Phys. Chem. C **116**, 8901 (2012).

[8] Q. Liu, B. Li, J. Liu, H. Li, Z. Liu, K. Dai, G. Zhu, P. Zhang, F. Chen, and J. Dai, Structure and band gap tuning of transparent $(Ba_{1-x}Sr_x)SnO_3$ thin films epitaxially grown on MgO substrates, Europhys. Lett. **98**, 47010 (2012).

[9] N. Alidoust, M. C. Toroker, J. A. Keith, and E. A. Carter, Significant reduction in NiO band gap upon formation of $Li_xNi_{1-x}O$ alloys: Applications to solar energy conversion, ChemSusChem **7**, 195 (2014).

[10] Y. Qu and X. Duan, Progress, challenge and perspective of heterogeneous photocatalysts, Chem. Soc. Rev. **42**, 2568 (2013).

[11] S. Yang, D. Prendergast, and J. B. Neaton, Tuning semiconductor band edge energies for solar photocatalysis via surface ligand passivation, Nano Lett. **12**, 383 (2012).

[12] Y. Li, Y.-L. Li, C. M. Araujo, W. Luo, and R. Ahuja, Single-layer MoS_2 as an efficient photocatalyst, Catal. Sci. Technol. **3**, 2214 (2013).

[13] H. L. Zhuang and R. G. Hennig, Single-layer group-III monochalcogenide photocatalysts for water splitting, Chem. Mater. **25**, 3232 (2013).

[14] Y. Yu, S.-Y. Huang, Y. Li, S. N. Steinmann, W. Yang, and L. Cao, Layer-dependent electrocatalysis of MoS_2 for hydrogen evolution, Nano Lett. **14**, 553 (2014).

[15] S. Yang, D. Prendergast, and J. B. Neaton, Strain-induced band gap modification in coherent core/shell nanostructures, Nano Lett. **10**, 3156 (2010).

[16] J. J. Mortensen, L. B. Hansen, and K. W. Jacobsen, Real-space grid implementation of the projector augmented wave method, Phys. Rev. B **71**, 035109 (2005).

[17] J. Enkovaara, C. Rostgaard, J. J. Mortensen, J. Chen, M. Dułak, L. Ferrighi, J. Gavnholt, C. Glinsvad, V. Haikola, H. A. Hansen, H. H. Kristoffersen, M. Kuisma, A. H. Larsen, L. Lehtovaara, M. Ljungberg, O. Lopez-Acevedo, P. G. Moses, J. Ojanen, T. Olsen, V. Petzold, N. A. Romero, J. Stausholm-Møller, M. Strange, G. A. Tritsaris, M. Vanin, M. Walter, B. Hammer, H. Häkkinen, G. K. H. Madsen, R. M. Nieminen, J. K. Nørskov, M. Puska, T. T. Rantala, J. Schiøtz, K. S. Thygesen, and K. W. Jacobsen, Electronic structure calculations with GPAW: a real-space implementation of the projector augmented-wave method, J. Phys.: Condens. Matter **22**, 253202 (2010).

[18] J. P. Perdew, A. Ruzsinszky, G. I. Csonka, O. A. Vydrov, G. E. Scuseria, L. A. Constantin, X. Zhou, and K. Burke, Restoring the density-gradient expansion for exchange in solids and surfaces, Phys. Rev. Lett. **100**, 136406 (2008).

[19] H. J. Monkhorst and J. D. Pack, Special points for Brillouin-zone integrations, Phys. Rev. B **13**, 5188 (1976).

[20] O. Gritsenko, R. van Leeuwen, E. van Lenthe, and E. J. Baerends, Self-consistent approximation to the Kohn-Sham exchange potential, Phys. Rev. A **51**, 1944 (1995).

[21] M. Kuisma, J. Ojanen, J. Enkovaara, and T. T. Rantala, Kohn-Sham potential with discontinuity for band gap materials, Phys. Rev. B **82**, 115106 (2010).

[22] I. E. Castelli, T. Olsen, S. Datta, D. D. Landis, S. Dahl, K. S. Thygesen, and K. W. Jacobsen, Computational screening of perovskite metal oxides for optimal solar light capture, Energy Environ. Sci. **5**, 5814 (2012).

[23] I. E. Castelli, J. M. García-Lastra, F. Hüser, K. S. Thygesen, and K. W. Jacobsen, Stability and bandgaps of layered perovskites for one- and two-photon water splitting, New J. Phys. **15**, 105026 (2013).

[24] I. E. Castelli, F. Hüser, M. Pandey, H. Li, K. S. Thygesen, B. Seger, A. Jain, K. A. Persson, G. Ceder, and K. W. Jacobsen, New Light-Harvesting Materials Using Accurate and Efficient Bandgap Calculations, Adv. Energy Mater., 1400915 (2014).

[25] F. Hüser, T. Olsen, and K. S. Thygesen, Quasiparticle GW calculations for solids, molecules, and two-dimensional materials, Phys. Rev. B **87**, 235132 (2013).

[26] R. W. Godby and R. J. Needs, Metal-insulator transition in Kohn-Sham theory and quasiparticle theory, Phys. Rev. Lett. **62**, 1169 (1989).

[27] P. Larson, M. Dvorak, and Z. Wu, Role of the plasmon-pole model in the GW approximation, Phys. Rev. B **88**, 125205 (2013).

[28] R. Shaltaf, G.-M. Rignanese, X. Gonze, F. Giustino, and A. Pasquarello, Band offsets at the Si/SiO_2 interface from many-body perturbation theory, Phys. Rev. Lett. **100**, 186401 (2008).

[29] We note that spin-orbit coupling has not been included in the calculations presented here. The absolute value of the band gap

of $CsPbI_3$ can therefore be expected to be about 1 eV larger than calculated here [31].

[30] The pseudo-Hartree potential close to an atomic core is calculated as the integral of the *s*-shaped compensation charge times the pseudo-Hartree potential, i.e., the soft part of the Hartree potential averaged using the *s* compensation charge as a weight function.

[31] I. E. Castelli, J. M. Garcia-Lastra, K. S. Thygesen, and K. W. Jacobsen, Bandgap calculations and trends of organometal halide perovskites, APL Mater. **2**, 081514 (2014).